

Discovery and development of macrocyclic peptide modulators of the cannabinoid 2 receptor

Nataša Tomašević,^[a] Fabiola Susanna Emser,^[a] Jasmin Gattringer,^[a] Simon Hasinger,^[a] Roland Hellinger,^[a] Peter Keov,^[b,c] Manuel Felkl,^[d] Jürg Gertsch,^[e] Christian F.W. Becker,^[d] and Christian W. Gruber^{*[a]}

^[a] Center for Physiology and Pharmacology, Institute of Pharmacology, Medical University of Vienna, 1090 Vienna, Austria

^[b] Monash Institute of Pharmaceutical Sciences, Monash University, Parkville, VIC, 3052, Australia

^[c] ARC Centre for Cryo-electron Microscopy of Membrane Proteins, Monash Institute of Pharmaceutical Sciences, Monash University, Parkville 3052, VIC, Australia

^[d] Institute of Biological Chemistry, Faculty of Chemistry, University of Vienna, 1090 Vienna, Austria

^[e] Institute of Biochemistry and Molecular Medicine, University of Bern, 3012 Bern, Switzerland

***Correspondence to** Christian W. Gruber, Email: christian.w.gruber@meduniwien.ac.at

cannabinoid type 2 receptor • plant • peptide • G protein-coupled receptor • allosteric modulator

ABSTRACT: The cannabinoid type 2 receptor (CB₂R), a G protein-coupled receptor (GPCR), is an important regulator of immune cell function and a promising target for to treat chronic inflammation and fibrosis. While CB₂R is typically targeted by small organic molecules, including endo-, phyto- and synthetic cannabinoids, peptides may offer a different interaction space, owing to their larger size and greater contact area they facilitate differential interactions with a specific receptor target. Here we explore plant-derived cyclic cystine-knot peptides as ligands of the CB₂R. Cyclotides are known for their exceptional biochemical stability. Recently they gained attention as modulators of GPCR signaling and as templates for designing peptide ligands with improved pharmacokinetic properties over linear peptides. Cyclotide-based ligands for CB₂R were profiled based on a peptide-enriched extract library comprising nine plant species. Employing pharmacology-guided fractionation and peptidomics we identified cyclotide vodo-C1 from sweet violet plant (*Viola odorata*) as a full agonist of CB₂R with an affinity (K_i) of 1 μM and a potency (EC₅₀) of 8 μM. Leveraging deep learning networks we verified the structural topology of vodo-C1 and modelled its molecular volume in comparison to the CB₂R ligand binding pocket. In a fragment-based approach we designed and characterized vodo-C1-based bicyclic peptides (vBCL1-4), aiming to reduce size and improve potency. Opposite to vodo-C1, the vBCL peptides lacked the ability to activate the receptor, but acted as negative allosteric modulators or neutral antagonists of CB₂R. This study introduces a new macrocyclic peptide phytocannabinoid, which served as template for the development of synthetic CB₂R peptide modulators. These findings offer opportunities for future peptide-based probe and drug development at cannabinoid receptors.

INTRODUCTION

The endocannabinoid system comprises the endogenous arachidic acid-derived ligands anandamide and 2-arachidonoylglycerol, enzymes facilitating endocannabinoid transport and metabolism, and importantly, the cannabinoid type 1 and 2 receptors (CB₁R and CB₂R). These G protein-coupled receptors (GPCRs) play a fundamental role in maintaining homeostasis in vertebrates across various physiological processes. Due to its expression in peripheral lymphoid tissues and cells of the immune system, the CB₂R emerged as a potential therapeutic target for numerous diseases including autoimmune disorders, metabolic conditions, cancer and chronic inflammatory disorders^{1,2}. Although considerable efforts have been made to develop CB₂R-selective therapeutics, none have yet reached the market, being unable to meet efficacy endpoints within clinical evaluation. High lipophilicity and poor target engagement of small molecule cannabinoid ligands are usually associated with high toxicity and unwanted side effects, whereas applying lower, tolerated doses results in lack of clinical efficacy³. Addressing the current challenges of cannabinoid modulators and chemical probes is crucial for advancing our understanding of CB₂R pharmacology and unlocking the therapeutic potential of this receptor⁴. Recently, peptides have gained attention as modulators of cannabinoid receptors, exemplified by the discovery of endogenous hemoglobin-derived peptide allosteric modulators of cannabinoid receptors⁵⁻⁷. As alternative to small molecule drugs, peptides offer potentially enhanced safety profiles^{8,9}, combining the potency and selectivity of larger biologics with more efficient and cost-effective production⁹. The increasing discoveries of peptide GPCR ligands in recent years has primarily been driven by advancements in computational biology¹⁰, structure-based design¹¹, virtual library screening¹², and rational design inspired by natural scaffolds¹³⁻¹⁵.

While *Cannabis sativa* L. produces the tetrahydrocannabinoid-type ligands, known as phytocannabinoids, also other cannabinoid receptor ligands from plants have been identified¹⁶. Notably, plants offer an extensive chemical space of bioactive peptides, with cyclotides evolving as innovative candidates for GPCR ligand discovery and design^{8,14,17-19}. These plant-derived peptides contain the structural feature known as cyclic cystine-knot motif²⁰, which sparked their use templates for the design of stable peptide-based therapeutics with an improved pharmacokinetic profile^{17,21,22}. Building on convenient and robust technologies that allow their (i) analytical characterization using peptidomics^{23,24}, (ii) automated access to correctly folded peptides via solid-phase chemistry²⁵, and (iii) access to rapid plate-based pharmacological screening assays¹⁸, in this study we aimed to explore cyclotide-containing plants to identify modulators of the CB₂R.

Using a pharmacology-guided fractionation workflow comprising nine peptide-enriched plant extracts we identified a cyclotide from sweet violet (*Viola odorata*) that displaced an orthosteric small molecule radioligand ([³H]-CP55940) from the binding site of CB₂R, and

activated the receptor, as determined by second messenger quantification. Based on the unique three-dimensional fold of this peptide, we designed and synthesized bicyclic analogs and provided comprehensive pharmacological characterization of these molecules at the CB₂R. Given their stability, these peptide ligands arising from this study will serve as novel research tools for dissecting cannabinoid receptor pharmacology and inspire future drug development.

RESULTS

Screening of a cysteine-rich peptide library to discover CB₂R ligands. Driven by the concept of nature-derived peptides as source for identification of new chemical scaffolds to modulate GPCR signaling^{8,17} we prepared a peptide-enriched plant extract library comprising nine plant species previously recognized to express a suite of cysteine-rich peptides. This included cyclotides from *Carapichea ipecacuanha*, *Palicourea tomentosa*, *Viola odorata*, and *Viola tricolor*^{26,27}, knottin-like peptides from *Bryonia alba*²⁸, *Salix alba* and *Strophanthus kombe*, as well as short protease inhibitor-like peptides from *Helianthus annuus*²⁹ and *Citrus limon*. Using chemical solvent and solid phase extraction, we generated a diverse library containing myriad of unknown or previously identified peptides and documented their mass signals in the range of 2,500-4,000 Da with matrix-assisted laser desorption ionization time-of-flight (MALDI-TOF) mass spectrometry (MS) analysis (**Supplementary Fig. 1**). First, we performed displacement of [³H]-CP55940 binding at human CB₂R stably expressed in CHO-K1 membranes by WIN55,212-2 to validate assay conditions (**Supplementary Fig. 2**). Subsequently, we screened the peptide library in radioligand displacement binding assays at the CB₂R (**Fig. 1a**). Only cyclotide-containing plant extracts were able to displace the CB₂R orthosteric small molecule radioligand agonist [³H]-CP55940, and the sweet violet extract (*V. odorata*) exhibited the most pronounced binding effect (**Fig. 1a,b**). To identify and isolate a CB₂R cyclotide ligand from *V. odorata*, we utilized a pharmacology-guided screening and purification approach. Preparative reversed-phase (RP) high performance liquid chromatography (HPLC) of *V. odorata* extract yielded six cyclotide-enrich fractions A-F (**Fig. 1c, Supplementary Fig. 3a-f**), which were assayed in radioligand binding experiments at CB₂R. Cyclotide-rich fractions A-D displayed none to moderate displacement of [³H]-CP55940 (70%-130% of radioligand bound), whereas fractions E and F (**Supplementary Fig. 3e-f**), exhibited the strongest ability to displace radioligand from the CB₂R (12% and 2% of radioligand bound, respectively) (**Fig. 1d**).

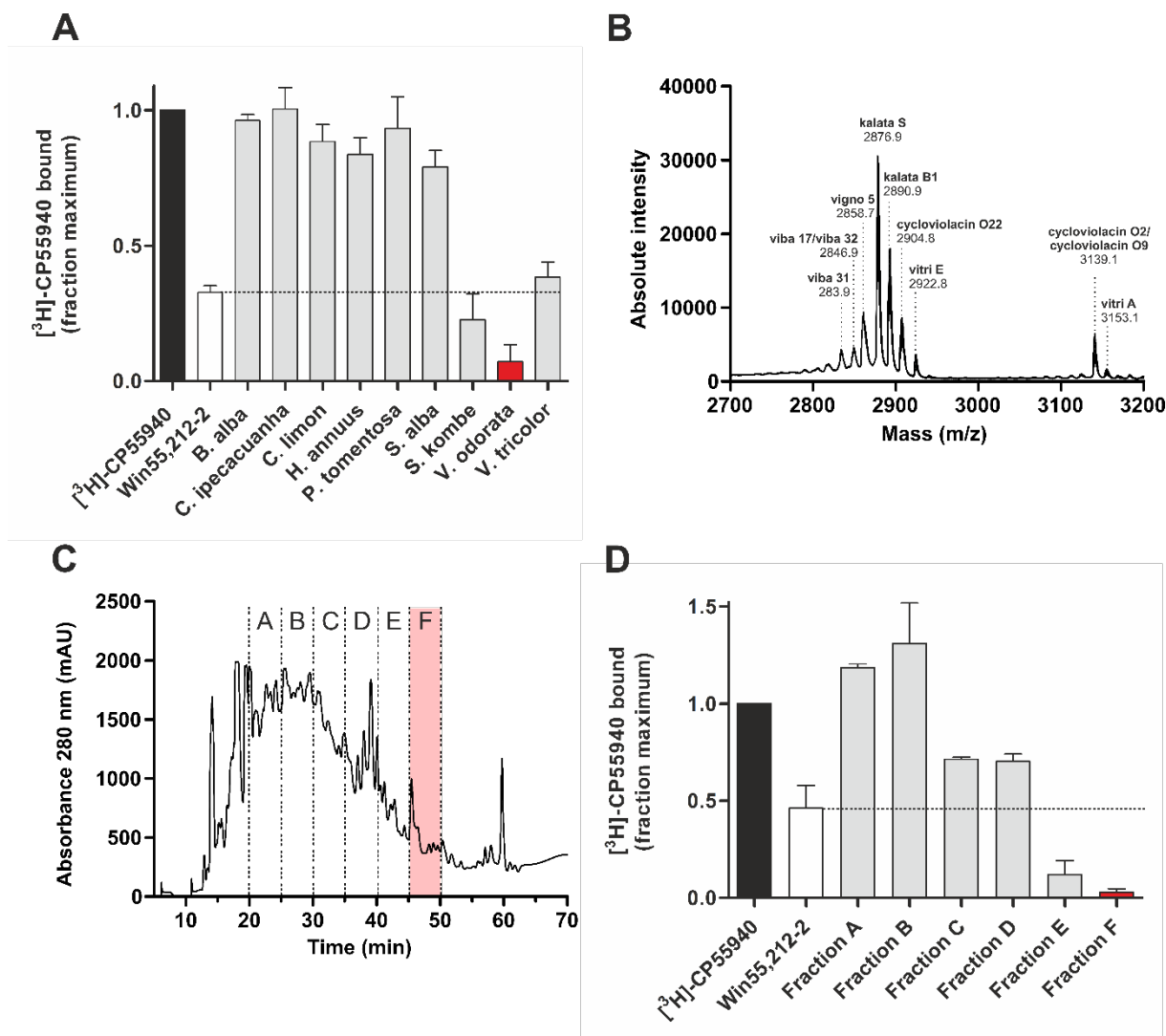


Figure 1. Screening of peptide-enriched plant extracts on CB₂R. (A) Binding assays utilizing radioligand displacement of [³H]-CP55940 (0.4 nM, black bar) by peptide-enriched plant extracts, i.e. *Bryonia alba*, *Carapichea ipecacuanha*, *Citrus limon*, *Helianthus annuus*, *Palicourea tomentosa*, *Salix alba*, *Strophanthus kombe*, *Viola odorata* and *Viola tricolor* (300 µg/mL, gray bars; extract of *V. odorata* was used for further purification, red bar) using human CB₂R-containing membrane preparations. WIN55,212-2 (10 nM, white bar) was used as positive control. (B) Mass spectrometry analysis (MALDI-TOF) of *V. odorata* extract with the major mass signals (>20% base peak intensity) shown as monoisotopic masses [M+H]⁺. Known peptide masses (± 1 m/z) were labelled with the corresponding cyclotide name published in CyBase³⁰. (C) Preparative RP-HPLC chromatogram of the peptide extract from *V. odorata* with the peptide-rich fractions (denoted as A-F) separated by dotted lines. (D) Radioligand displacement binding of [³H]-CP55940 (0.4 nM, black bar) by semi-purified peptide fractions A-F (300 µg/mL, gray bars; fraction F was used for further purification, red bar) using human CB₂R containing membrane preparations. Specific binding was obtained by subtracting of non-specific from total binding. Data are presented as mean ± SEM (n=3) and are normalized to the fraction of maximum bound radioligand, which refers to an average of 4,500-5,000 fmoles/mg protein for CB₂R.

Identification of the CB₂R ligand vodo-C1 from *V. odorata*. We next examined the cyclotide content of fraction F, which exhibited the strongest displacement of radioligand at CB₂R. MALDI-TOF and analytical HPLC analysis of fraction F revealed the presence of nine known cyclotides^{30,23} (**Supplementary Fig. 3f, Supplementary Table 1**) and one previously unidentified peptide with a molecular weight of 3432.2 Da. Since *V. odorata* is a well-

documented cyclotide-expressing plant³¹ we assumed the unknown peptide, which was named vodo-C1, is also a cyclotide. Hence, we first applied a chemical derivatization approach to determine the cysteine content of vodo-C1.

Chemical reduction of the (putative) disulfide bonds by dithiothreitol (DTT) and *S*-carbamidomethylation of cysteines with iodoacetamide revealed a shift from 3432.1 Da (native) to 3438.1 Da (reduced) and 3780.2 Da (alkylated), resulting in mass difference of +6 Da and +348 Da, respectively, which corresponds to a peptide containing six cysteine residues (i.e. three disulfide bonds) (**Fig. 2a**). To elucidate the amino acid sequence of this peptide and to determine if the backbone is cyclized, the *S*-carbamidomethylated peptide was enzymatically processed with endoprotease GluC (EndoGluC), trypsin and chymotrypsin and subsequently analyzed by mass spectrometry. EndoGluC proteolytic digest revealed a mass peak of 3798.4 Da, which corresponds to an increase of +18.2 Da due to hydrolysis of the *S*-carbamidomethylated peptide. This suggested 'ring-opening' of the peptide by hydrolysis, which is a main feature of cyclotides²⁶.

Two additional fragments have been identified in this digest with masses of 1252.4 Da and 2564.9 Da, indicating additional cleavage of the linear precursor at Glu residues (**Fig. 2b**). Each of the tryptic and chymotryptic digests yielded two cleavage products of the linear precursor, with masses of 1652.6 Da and 2164.8 Da, and 628.2 Da and 3189.2 Da, respectively (**Supplementary Fig. 4a & 5a**). The above identified proteolytic cleavage products were subjected to collision-induced fragmentation by MALDI-TOF MS/MS. The resulting MS/MS spectra were manually annotated for their N-terminal b- and C-terminal y-ion series (**Fig. 2b-c, Supplementary Fig. 4b-c & 5b-c**). The integration of sequence data from these different proteolytic experiments enabled a complete assignment of the peptide sequence, which is cyclo-GDPLPCGETCFTGKCYSETIGCTCEWPICTKN. In addition, fragment analysis of the trypsin digest allowed distinction between isobaric residues Gln/Lys (**Supplementary Fig. 4b-c**), and the chymotrypsin digest was employed to distinguish between isobaric Leu/Ile (**Supplementary Fig. 5b-c**). Finally, the sequence of vodo-C1 was confirmed by high-sensitivity amino acid analysis and sequence similarity analysis³⁰ (**Supplementary Fig. 6, Supplementary Table 2**).

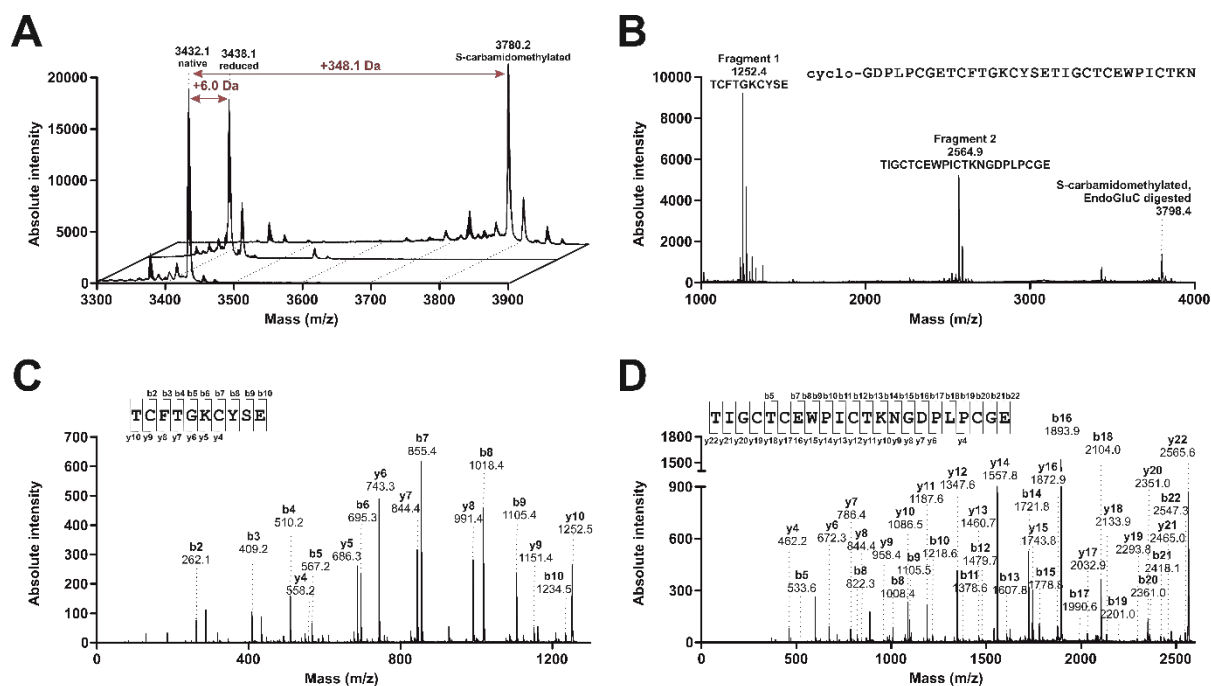


Figure 2. Identification and amino acid sequence elucidation of cyclic disulfide-rich peptide from *V. odorata*. (A) MALDI-TOF mass spectrum of native (3432.1 Da), reduced (3438.1 Da) and S-carbamidomethylated peptide (3780.2 Da) revealed mass shifts of +6.0 Da after and +348.1 Da, observed after DTT- reduction and S-carbamidomethylation, respectively. (B) MALDI-TOF spectrum of S-carbamidomethylated full-length vodo-C1 peptide after digestion with EndoGluC. All labeled peaks refer to monoisotopic masses [M+H]⁺. In total, two fragments were detected indicating cleavage of the peptide at two distinct positions. (C) MS/MS spectrum of the mass 1252.5 Da and (D) the mass 2565.6 Da precursor with identified fragment b- and y- ions labeled (monoisotopic [M+H]⁺).

Synthesis of vodo-C1 and pharmacological characterization reveals CB₂R full agonism. Following *de novo* sequencing, vodo-C1 was chemically synthesized for pharmacological characterization. A combination approach using fluorenyl-methoxycarbonyl (Fmoc) chemistry, followed by N-to-C-terminal backbone cyclization using peptide hydrazide as thioester precursor and subsequent oxidative folding yielded the cyclotide vodo-C1 (**Supplementary Fig. 7a-c**). Its native disulfide configuration was confirmed by analytical HPLC co-elution analysis in that synthetic and plant-extracted vodo-C1 produced a single peak at 38.9 min (**Fig. 3a**). Subsequently, vodo-C1 was subjected to concentration-dependent binding studies and second messenger quantification at the CB₂R. Compared to CP55940, a full reference agonist of the CB₂R³², vodo-C1 displaced [³H]-CP55940 in a concentration-dependent manner with a K_i value of 0.9 ± 0.1 μM (**Fig. 3b**). Functional cAMP assay revealed that vodo-C1 activated CB₂R, with an E_{max} of 102.8 ± 4.1% and an EC₅₀ of 7.8 ± 1.0 μM (**Fig. 3c**). These data suggest that vodo-C1 is a full agonist of CB₂R and more importantly, it is the first identified peptide agonist of CB₂R.

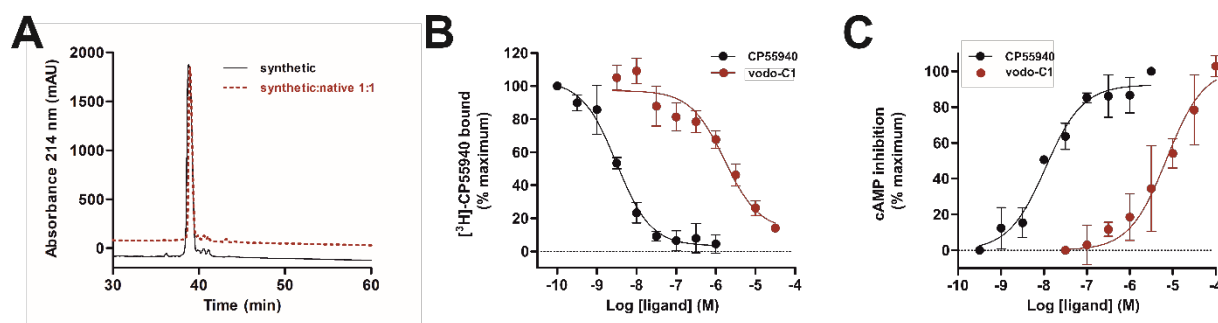


Figure 3. Pharmacology of synthetic vodo-C1 cyclotide. (A) Quality control of synthesized vodo-C1 (black signal) analyzed by RP-HPLC (purity > 95%) with retention time of 38.8 min and co-elution experiment of native and synthetic vodo-C1 (ratio 1:1; red dashed signal) showing one single peak at 38.9 min. (B) Radioligand displacement of [³H]-CP55940 (0.3 nM) by synthetic vodo-C1 (red circles) using human CB₂R containing membrane preparations led to a calculated affinity (K_i) of $0.9 \pm 0.1 \mu\text{M}$. CP55940 was used as a positive control (black circles). Data are presented as mean \pm SEM and are normalized to the percentage of maximum binding, which refers to an average of 4,500-5,000 fmoles/mg protein for CB₂R ($n=3$). (C) Concentration-dependent cAMP inhibition following full receptor activation by synthetic vodo-C1 (red circles) in CHO-K1 cells stably expressing the human CB₂R with EC_{50} value of $7.8 \pm 1.0 \mu\text{M}$ and E_{max} of $102.8 \pm 4.1\%$. CP55940 was used as a positive control (black circles; $n=3$).

Vodo-C1-inspired design of cannabinoid receptor ligands. To better understand the interaction of the cyclotide ligand with the receptor, we modelled vodo-C1 using AlphaFold³³, combined with workflow for structure prediction and design of cyclic peptides³⁴. The cyclotide has a typical Möbius fold given the presence of a cis-prolyl peptide bond in loop 5, which causes a twist in the circular backbone²⁷ and a cyclic peptide backbone with three disulfide bonds (connectivity: C_I-C_{IV}, C_{II}-C_V, C_{III}-C_{VI}) (Fig. 4a). Besides one conserved glutamic acid residue in loop 1³⁵, there are an additional two Glu residues in loops 3 and 5. This is an unusual feature since the majority of cyclotides contain one conserved glutamic acid residue²⁶. Hitherto, only five cyclotides have been identified with three Glu residues, including cliotide T2³⁶, tricyclon B³⁷, viba 14³⁸, hyfl B and hyfl C³⁹, making vodo-C1 one of the cyclotides with this unique amino acid composition. Overall, the model displayed predicted local distance difference test (pLDDT)-score with high confidence (pLDDT = 0.947) and a predicted aligned error between 0 and 15 for all residues (Supplementary Fig. 8a-b). Vodo-C1 aligned with the prototype cyclotide structure of kalata B1 with a root mean squared deviation (RMSD)-value of 0.648 Å (Fig. 4b). Residues in loop 2 (Phe11) and loop 5 (Thr26 and Ile28) form a hydrophobic patch with a calculated hydrophobicity index of 2.77 (according to the hydrophobicity scale by Eisenberg⁴⁰) (Fig. 4c). Furthermore, we calculated the molecular volumes of vodo-C1 in comparison to kalata B1, and other cannabinoid CB₂R ligands (Supplementary Table 3). Vodo-C1 has a volume of 3516 Å³, whereas the CB₂R binding pocket has a calculated volume ranging from approximately 415 to 447 Å³ 41.

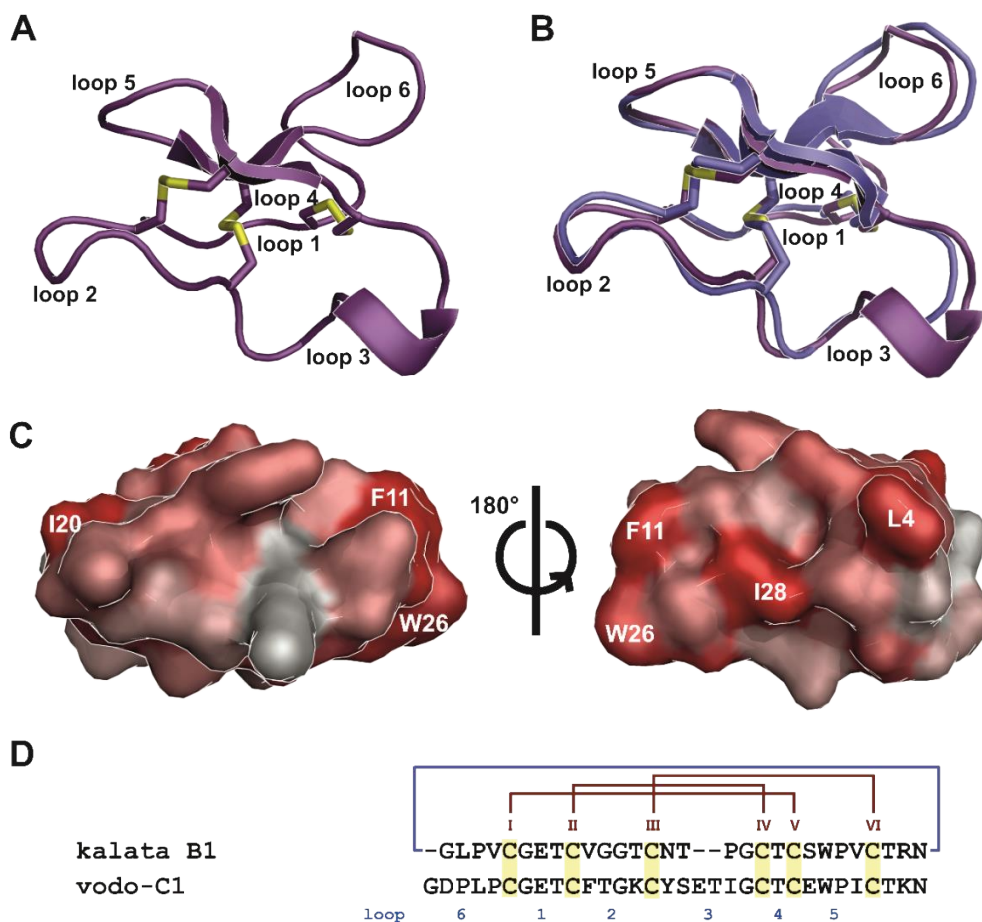


Figure 4. Structure prediction of native vodo-C1 using AfCycDesign. (A) A cartoon representation of predicted structure of cyclotide vodo-C1. The sulfur atoms of the six cysteine residues are highlighted in yellow. (B) A structural alignment of kalata-B1 (PDB ID: 1NB1) and vodo-C1 using PyMol. An RMSD-value of 0.648 Å was calculated for the alignment of the two peptides. (C) A surface representation of vodo-C1. A hydrophobicity scale according to Eisenberg³² was applied to the model. Hydrophobic residues are highlighted in red, whereas hydrophilic residues are shown in white. Hydrophobic residues (L4, F11, I20, W26, I28) are highlighted in white. (D) Sequence alignment of vodo-C1 with kalata B1. Conserved cysteine residues (I-IV) are highlighted in yellow and labelled with Roman numbers (in red) above the alignment, whereas cyclotide loops (1-6) connecting different cysteine residues are labelled with Arabic numbers (in blue) under the alignment.

Given the bulky size of cyclotides, we hypothesized a smaller surface area and volume of vodo-C1-inspired shorter peptides would enable better penetration of the binding pocket of the receptor and exhibit increased affinity and/or potency¹³. Therefore, in a fragment-based approach we designed four smaller, bicyclic peptides using the native sequence of vodo-C1 as template termed vodo-C1-inspired bicyclic loops 1-4 (vBCL1-4) peptides (**Fig. 5a**). We synthesized linear peptides, each composed of two native vodo-C1 loops and three cysteine residues: vBCL1 (loops 1 and 2, containing 10 residues), vBCL2 (loop 2 and 3, containing 13 residues), vBCL3 (loop 5 and 6, containing 15 residues), and vBCL4 (loop 6 and 1, containing 14 residues). Loop 4 was excluded since it comprises a single amino acid residue. Cyclization was achieved by using the 1,3,5-tris-(bromomethyl)-benzene⁴², which contains three thio-reactive groups able to couple with three cysteine moieties of each of linear peptides. (**Fig. 5b, Supplementary Fig. 9a-d**).

Next, we determined the molecular pharmacological properties of vBCL peptides to obtain information regarding their affinity and functional effects at CB₂R. The peptides were measured in two-point displacement radioligand assays at CB₂R. vBCL1 and 2 (10 μM) exhibited weak displacement of [³H]-CP55940 from CB₂R (75%-90% radioligand bound), whereas vBCL3 and 4 (100 nM and 10 μM, respectively) did not bind to the receptor (**Supplementary Fig. 10a**). The functional cAMP assays confirmed that all four vBCLs did not activate the human CB₂R at concentrations up to 30 μM (**Supplementary Fig. 10b**). To determine whether any of the vBCLs would be able to bind to CB₁R, we performed single-point displacement radioligand assay on HEK293 membranes transiently expressing rat CB₁R. Importantly, the peptides did not displace [³H]-CP55940 from CB₁R at concentrations of 10 μM (**Supplementary Fig. 10c**).

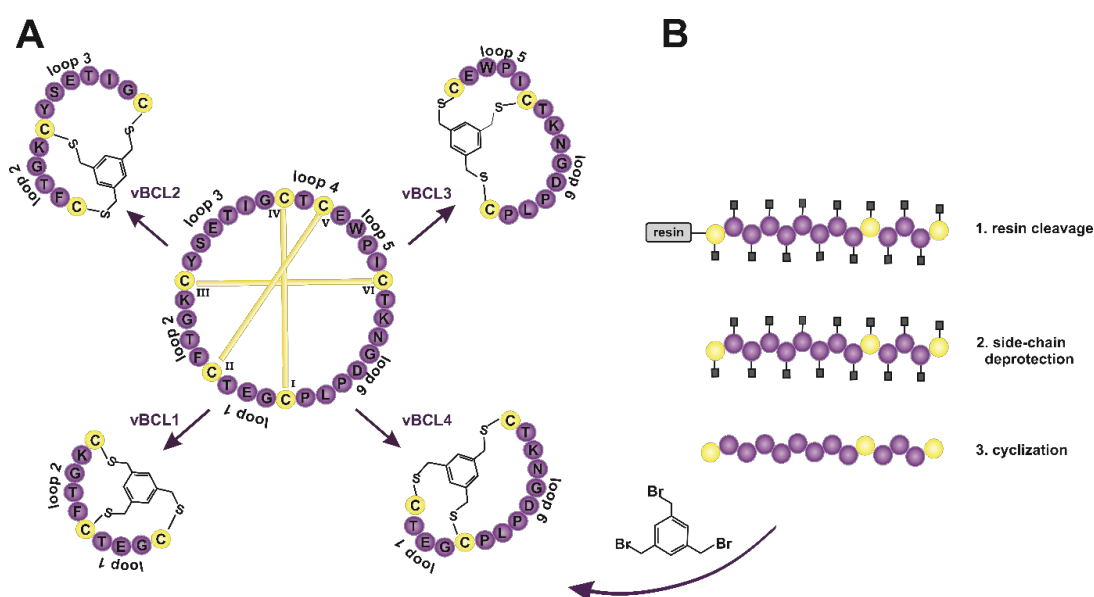


Figure 5. Schematic illustration of design and synthesis strategy of novel bicyclic peptides to target CB₂R. (A) Fragment-based design of bicyclic peptides vBCL1-4, each comprising two loops of native vodo-C1 cyclotide. (B) Peptide preparation via solid phase peptide synthesis and cyclization by coupling the Heinis reagent 1,3,5-tris-(bromomethyl)-benzene, containing three thio-reactive moieties that reacted with the three thiol groups of the cysteine residues of each linear peptide.

Cyclotide-derived bicyclic peptides vBCL1-4 are distinct CB₂R modulators with allosteric properties. Given the observed lack of strong radioligand displacement and activation of the CB₂R, we screened vBCLs for allosteric properties at CB₂R using functional second messenger assays. By measuring CB₂R-mediated inhibition of cellular cAMP production, we demonstrated that 10 μM vBCL2 and vBCL4 decreased the potency (EC₅₀) of the full agonist CP55940 by approximately 5-fold from 15 nM to 80 nM and 84 nM, respectively. In contrast, the shift in CP55940 potency with 10 μM of vBCL1 or vBCL3 was weaker (~2-fold for each). However, it is important to note that vBCL3 and vBCL4 both led to reduction in basal response. Additionally, vBCL3 also decreased the efficacy of CP55940 by ~40% (E_{max} = 61%) (**Fig. 6a, Supplementary Table 4**). Based on their effects on CP55940 activity, the distinct effects of peptides vBCL2-4 were further analyzed in more detail.

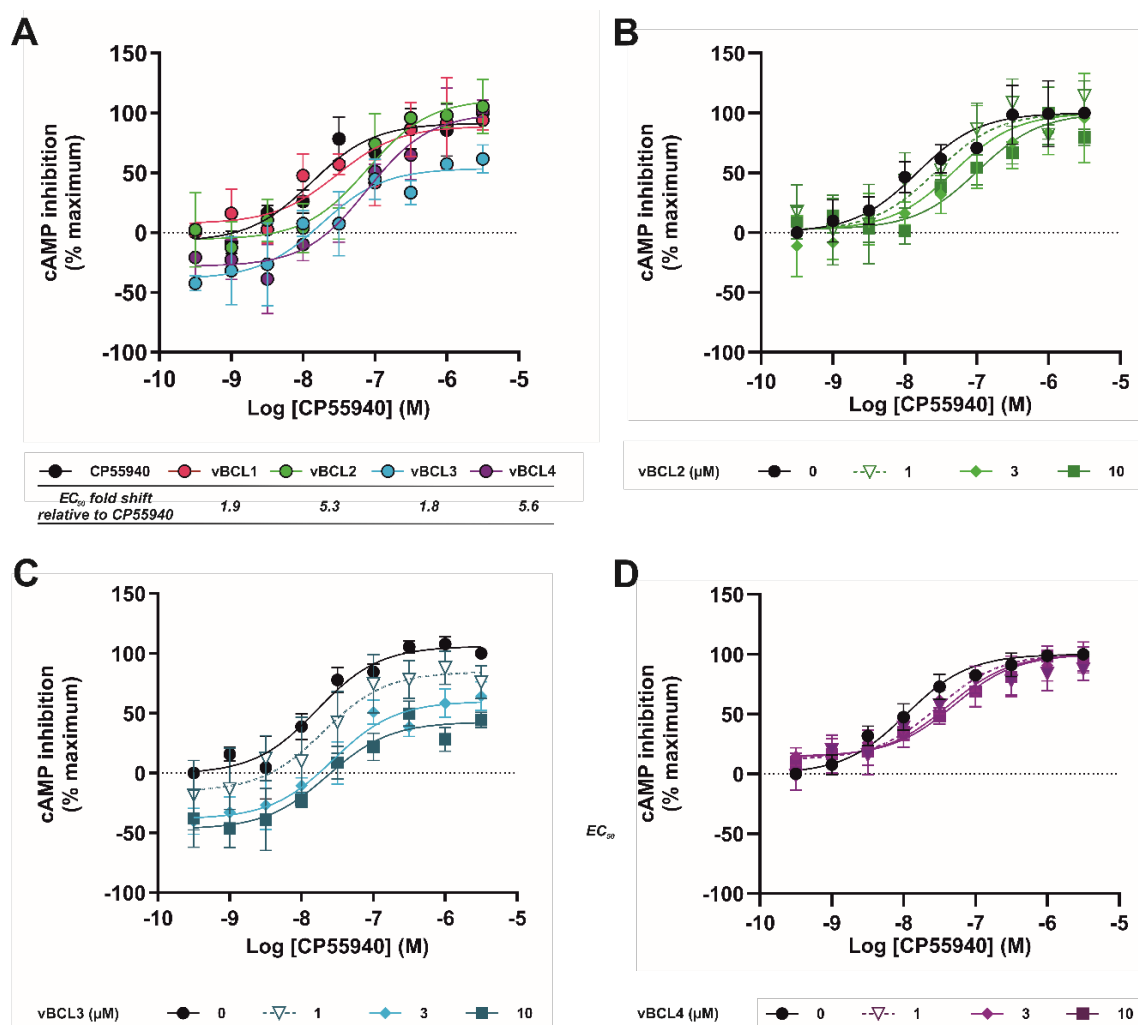


Figure 6. Allosteric effects of vBCL1-4 on CP55940 concentration-response curves at the CB₂R. (A) Functional cAMP assay of 10 μ M vBCL1 (red circles), vBCL2 (green circles), vBCL3 (blue circles), and vBCL4 (violet circles) co-incubated with increasing concentrations of CP55940 agonist in CHO-K1 cells stably expressing CB₂R. Calculated fold change of CP55940 EC_{50} for each vBCL is presented as table insert. Dose-dependent allosteric modulation of CP55940 concentration-response curve in presence of 1 μ M (inverted triangles), 3 μ M (diamonds) and 10 μ M (squares) of (B) vBCL2 (green), (C) vBCL3 (blue) and (D) vBCL4 (violet). Data are normalized to percentage of maximal activation, detected at the highest CP55940 concentration, and are shown as mean \pm SEM of 3-4 independent experiments.

To examine whether these effects observed are concentration-dependent, we tested concentrations of 1 μ M, 3 μ M and 10 μ M of vBCL2-4 (Fig. 6b, Supplementary Table 5). The observed dextral shift of the CP55940 concentration-response curve by increasing concentrations of vBCL2 was best fit using the Gaddum/Schild EC_{50} nonlinear regression model indicative of competitive antagonism with an estimated functional affinity of \sim 1.6 μ M ($pA_2 = 5.8 \pm 0.3$; Supplementary Table 7). This agrees with the partial displacement of [³H]-CP55940 induced by vBCL2 (Supplementary Fig. 10a). vBCL4 behaved similar to vBCL2, inducing a decrease of the CP55940 potency (Fig. 6d, Supplementary Table 5). However, this concentration-dependent inhibition appeared saturable and was best fit using the operational model of allosterism, yielding an estimated affinity of \sim 309 nM ($pK_B = 6.5 \pm 0.6$; Table 1).

Table 1. Analysis of vBCL4 concentration-dependent inhibition of CP55940- or WIN55,212-2- mediated cAMP formation at CB₂R

Agonist	vBCL4			
	log($\alpha\beta$) ^a	pK _B ^{a,b}	pA2 ^c	Slope ^c
CP55940	-0.63 ± 0.2	6.5 ± 0.6 (309 nM)	5.7 ± 1.0 (2.0 μM)	0.3 ± 0.3
WIN55,212-2	-1.03 ± 0.4	6.2 ± 0.4 (646 nM)	n.d.	n.d.

^a Values estimated via operational model of allosterism and agonism (equation 1) from data presented in Figures 6d and 7d

^b negative logarithm of molar affinity estimate; statistical significance was analyzed using an unpaired t test ($p > 0.05$)

^c Values estimated via Gaddum/Schild equation

Data are presented as means ± SEM of 3-4 individual experiments.

Co-incubation of vBCL3 (1 μM and 3 μM) marginally altered the potency of CP55950 but induced downward shifts of the CP55940 concentration-response curve reducing the efficacy from 100% to ~80% and 86%, respectively (**Fig. 6c, Supplementary Table 5**). Importantly, the basal activity was also reduced, and therefore operational model analysis was not possible. To validate that the observed reduction of basal activity mediated by vBCL3 is not due to potential intrinsic inverse agonism, we studied the effect of vBCL3 on CP55940 activity in the absence of forskolin (a known activator of adenylyl cyclase⁴³). CB₂R is known for its constitutive activity, which leads to the basal inhibition of adenylyl cyclase^{44,45}. We hypothesized that in the absence of forskolin, inverse agonism would reduce the constitutive activity of CB₂R and enhance the production of cAMP. Firstly, we confirmed that the assay system is sensitive to detect inverse agonism by measuring effects of varying concentrations of inverse agonist SR144528⁴⁵, which reduced the basal levels of CB₂R activity (**Supplementary Fig. 11a**). In the absence of forskolin, neither CP55940 alone, nor CP55940 co-incubated with vBCL3 yielded any effect on cellular cAMP levels (**Supplementary Fig. 11b**), concluding that vBCL3 lacks intrinsic inverse agonist activity.

Lastly, possible probe-dependent effects of all four vBCL peptide analogs were characterized, by extending the functional assays with the potent synthetic CB₂R full agonist WIN55,212-2 and the endocannabinoid 2-arachydonylglycerol (2-AG)³². Specifically, co-incubation of vBCL1 and vBCL3 peptide at 10 μM with WIN55,212-2 or 2-AG, respectively, resulted in EC₅₀ shifts of ~6-fold (**Fig. 7a-b, Supplementary Table 4**). Interestingly, vBCL3 induced both rightward and downward shifts of the WIN55,212-2 concentration-response curve, modulating the agonist potency (EC₅₀) from 1.5 nM to 9.4 nM and the maximal response (E_{max}) from 100% to ~54%. Furthermore, vBCL3 also reduced the basal activity of WIN55,212-2. On the other hand, vBCL2 and vBCL4 had larger effects on agonist potencies. Co-incubation of vBCL2 and vBCL4 peptide at 10 μM with 2-AG yielded EC₅₀ shifts by ~9-12 fold, from 480 nM to 4.4 μM and 5.9 μM, respectively. Also, treatment with 10 μM vBCL2 and vBCL4 shifted the EC₅₀ of WIN55,212-2 by approximately 29-fold and 75-fold, from 1.5 nM to 47 nM and 120 nM, respectively (**Fig. 7a-b, Supplementary Table 4**).

Given the interesting properties of vBCL3 (reduction of efficacy) and vBCL4 (greatest shift in potency), we further assessed the concentration-dependent effects of these two peptides when co-incubated with WIN55,212-2 (1 μ M, 3 μ M and 10 μ M). Similarly to their co-incubation with CP55940, vBCL3 and vBCL4 induced concentration-dependent rightward and downward shift of the WIN55,212-2 concentration-response curve (**7c-d**, **Supplementary Table 6**). Operational model analysis was not possible for vBCL3, but vBCL4 was best fit using the operational model for allosterism, rather than Schild regression (slope <1), exhibiting an affinity of \sim 646 nM ($pK_B = 6.2 \pm 0.4$; **Table 1**). Functional cooperativity analysis ($\log\alpha\beta$) between CP55940 and WIN55,212-2 for vBCL4 displayed \sim 2.5-fold difference, indicating probe-dependent allosteric modulation of CB₂R with these two agonists, albeit this was not significantly different.

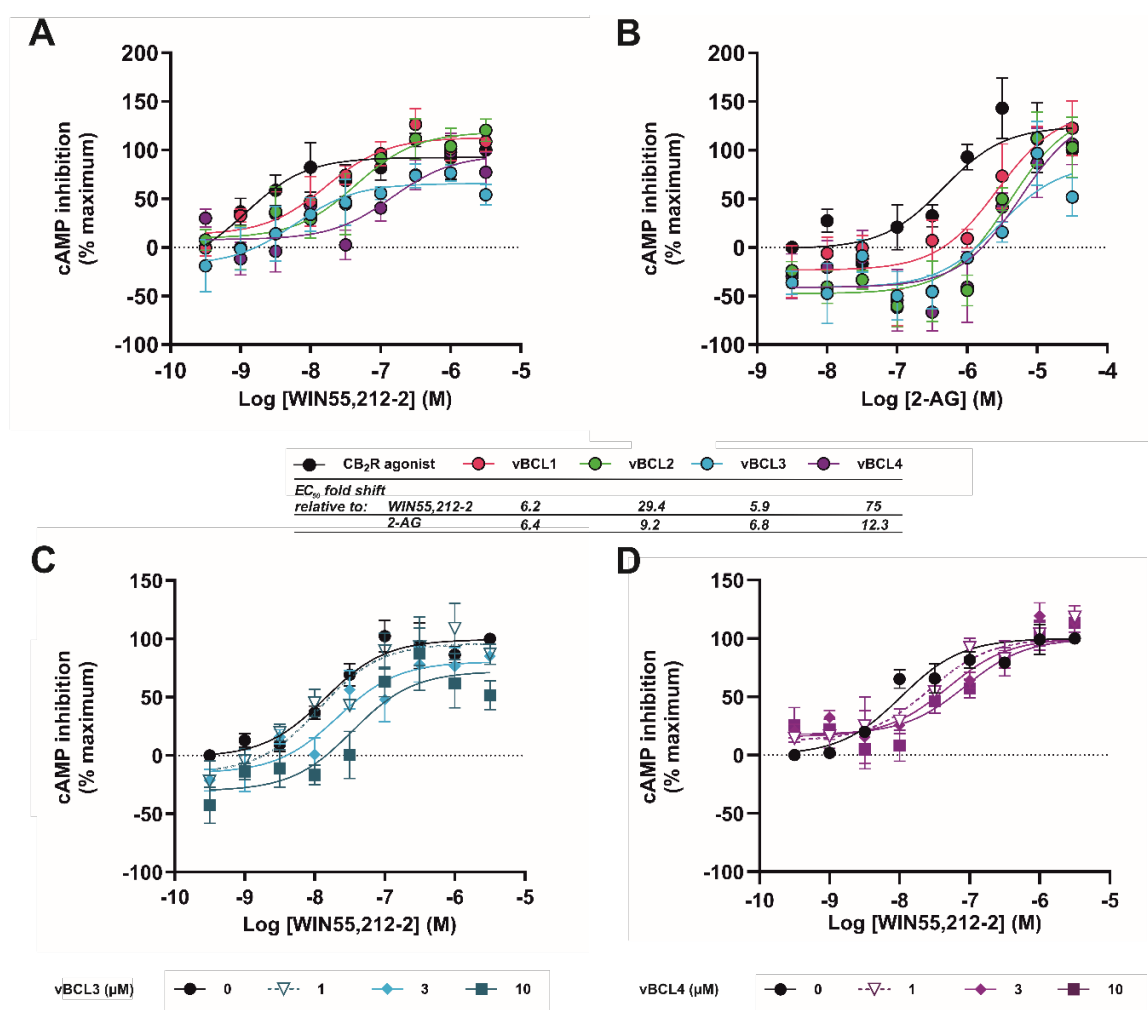


Figure 7. Allosteric effects of vBCL1-4 on WIN55,212-2 and 2-AG concentration-response curves at the CB₂R. Functional cAMP assay of 10 μ M vBCL1 (red circles), vBCL2 (green circles), vBCL3 (blue circles), and vBCL4 (violet circles) co-incubated with increasing concentrations of (A) WIN55,212-2 and (B) endogenous 2-AG in CHO-K1 cells stably expressing CB₂R. Calculated fold change of WIN55,212-2 and 2-AG EC_{50} for each vBCL is presented as table insert. Dose-dependent allosteric modulation of WIN55,212-2 concentration-response curve in presence of 1 μ M (inverted triangles), 3 μ M (diamonds) and 10 μ M (squares) of (C) vBCL3 (blue) and (D) vBCL4 (violet). Data are normalized to percentage of maximal activation, detected at the highest CP55940 concentration, and are shown as mean \pm SEM of 3-4 independent experiments.

In summary, all four bicyclic peptides attenuated agonist-mediated cAMP inhibition of WIN55,212-2, 2-AG and CP55940 albeit the effect was weaker in combination with CP55940. Detailed evaluation of the data suggests that vBCL4 is a negative allosteric modulator (NAM) on CP55940-, WIN55,212-2- and 2-AG-mediated inhibition of cAMP formation upon activation of CB₂R. Further, vBCL4 may be probe-dependent with the strongest effects observed for WIN55,212-2. Quantitative allosteric analysis was not possible for vBCL3 due to the insignificant effects on the EC₅₀-shift of CP55940 and WIN55,212-2 and observed reduction in basal activity. Based on our data vBCL2 (and vBCL1) may be best described as allosteric modulators of CB₂R, similar to vBCL4, whereas their lack of functional activation of CB₂R and partial displacement of radioligand in binding assays is also consistent with weak competitive (neutral) antagonism.

DISCUSSION

Pharmacological targeting of CB₂R holds significant therapeutic potential for autoimmune diseases, (neuro-)inflammation, fibrosis, and chronic inflammatory pain^{1–3,46,47}. Our objective was to identify peptide ligands for this GPCR. Motivated by the chemical diversity and unique physicochemical properties inherent to nature-derived peptides as a reliable source of GPCR ligands we systematically screened a custom library of cysteine-rich plant peptides to uncover modulators of CB₂R signaling^{13,18,19,48}. Employing a robust pharmacology-guided fractionation approach led to the discovery of the peptide vodo-C1 from the sweet violet (*V. odorata*) as a novel CB₂R peptide agonist. The cyclotide-inspired design of bicyclic peptides vBCL1-4 based on the naturally occurring vodo-C1 sequence found in *Viola* spp. yielded novel probes with NAM properties at CB₂R signaling.

GPCRs stand out as the leading drug target class⁴⁹. Typical approaches to identify GPCR-targeting peptide ligands involve high-throughput screening methods⁵⁰, in silico-genome mining⁵¹, molecular grafting of stabilized peptide scaffolds^{14,52} and de novo-design¹⁰. Since cannabinoid GPCRs, especially CB₂R, are targeted by natural products including Δ^9 -tetrahydrocannabinol and its derivatives, fatty acid derivatives from *Echinacea* spp.⁵³, or the widespread plant sesquiterpene β -caryophyllene⁵⁴, among others, we utilized a peptide-enriched plant extract library screening approach. This led to the isolation and characterization of a peptide cannabinoid from sweet violet that showed a CB₂R full agonism.

Herbal preparations of sweet violet have been used in Persian and Indian ethnomedicine for centuries, particularly in treatment of pain, respiratory- and intestinal inflammation, and cancer^{55,56}. In-depth investigations of *V. odorata* have acknowledged its expression of a variety of different cyclotides^{35,57}. Still we identified and characterized a hitherto unknown cyclotide from this violet species leveraging peptidomics²³ and computer-assisted modelling³⁴. The larger volume of cyclotides, approximately eight times that of endogenous 2-AG and other cannabinoids, may account for the moderate affinity and potency of vodo-C1 at CB₂R. The bulkier size might impede deep penetration of the receptor binding-core¹⁷ (~415-447 Å³), ideally suited for binding of small molecule cannabinoid ligands⁴¹. Peptide ligands of cannabinoid receptors like vodo-C1, including the recently discovered venom peptides that target CB₁R⁵⁸ may preferably interact with the extracellular regions of the binding pocket. While molecular details of peptide-ligand interaction with the CB₂R remain speculative, the identification of vodo-C1 as a plant-derived peptide CB₂R agonist expands the list known phytocannabinoids. The use of cyclopeptides offers opportunities for the development of novel CB receptor-selective peptide cannabinoid ligands. Moreover, peptide ligands like vodo-C1 and vBCL1-4 may inspire the development of probes to delineate the mode of action of peptide endocannabinoids (Pepcans), in particular pepcan-12 (RVD-hemopressin), which is generated from hemoglobin 2 via the pro-peptide pepcan-23^{59,60}.

Although the exact modes of action of pepcans (hemopressins) remain unclear, Bauer *et al.* have shown that pepcan-12 (RVD-hemopressin) can exert opposite allosteric effects at CB₁R and CB₂R, respectively⁶¹. The allosteric binding sites in CB₂R have recently gained attention⁷, particularly with endogenous signaling molecules like hemopressins exhibiting potential antinociceptive effects^{6,61}. Building on the concept of miniaturization of cyclotide derivatives¹³, the design of bicyclic vodo-C1-inspired peptides (vBCL1-4) using a fragment-based approach yielded potent GPCR modulators with allosteric properties toward CB₂R signaling, albeit unexpected. In fact, similar effects have been described for the phytocannabinoids (-)-trans- Δ^9 -tetrahydrocannabinol and (-)-cannabidiol at CB₁R. These two compounds are naturally synthesized from the common precursor cannabigerolic acid and are chemical isomers. While cannabidiol is bicyclic, tetrahydrocannabinol contains an additional benzene ring⁶². Despite the structural similarities, tetrahydrocannabinol and cannabidiol exert distinct neurochemical effects in the brain and their mechanisms of action on CB₁R differ markedly. While psychotropic tetrahydrocannabinol is a partial agonist of CB₁R, cannabidiol was identified as NAM of CB₁R, devoid of any psychotropic effects^{63,64}. By similarity, the plant-derived cyclotide is an agonist of CB₂R, while the bicyclic peptide analogs are NAMs of CB₂R.

The promising avenue of allosteric modulation in drug development has gained attention for its enhanced specificity and drug action^{65,66}. Investigating the impact of vBCL peptides at CB₂R, we observed the reduction in potency and efficacy of synthetic and endogenous agonists. Interestingly, allosteric modulation by certain peptides is probe-dependent, highlighting the importance of selecting orthosteric probes for screening of allosteric modulators at CB₂R and other GPCRs in the future. Notably, allosteric modulators of CB₂R, like synthetic EC21a, have shown therapeutic potential, in several animal models^{67,68}, indicative of the growing significance of allosteric modulation as an approach for targeting GPCRs. Specifically, it may offer an alternative strategy for enhancing cannabinoid receptor subtype selectivity of CB₂R.

In summary, we've unveiled a novel phytocannabinoid peptide that acts as a full agonist at CB₂R, underscoring the untapped potential of nature, particularly of plant-derived peptides, as a valuable source for GPCR drug discovery. Intriguingly, the design of cyclotide-inspired bicyclic peptides led to an unexpected transformation of the molecular mode of action from an agonist to the discovery of modulators with negative allosteric and neutral antagonist properties for CB₂R. These peptides offer valuable tools for delving into cannabinoid receptor pharmacology and lay the foundation for future developments in allosteric peptide-based cannabinoid ligands, promising desired pharmacological properties.

EXPERIMENTAL SECTION

Materials. Radioligand [³H]-CP55940 was obtained from PerkinElmer (Boston, MA, USA). 2-Arachidonoylglycerol, AM630, CP55940 and (R)-(+)-WIN55,212-2 mesylate salt, ammonium hydrogen bicarbonate (NH₄HCO₃), polyethylenimine (PEI), tris(hydroxymethyl) aminomethane (Tris), magnesiumchlorid hexahydrat (MgCl₂), forskolin, 3-Isobutyl-1-methylxanthine (IBMX), fatty acid-free bovine serum albumin (BSA), ethylenediaminetetraacetic acid (EDTA), α-cyano-hydroxy cinnamic acid (α-CHCA), and cell culture media and supplements were obtained from Sigma-Aldrich Chemicals (St. Louis, MO, USA). Acetonitrile (AcN), methanol (MeOH), dichloromethane (DCM), trifluoroacetic acid (TFA) were obtained as HPLC grade from Carl Roth (Karlsruhe, Germany). Endoprotease Glu-C, trypsin and chymotrypsin were purchased from New England Biolabs (Ipswich, MA, USA). All other chemicals were of analytical grade and obtained from standard commercial sources. The jetPRIME transfection reagent was obtained from Polyplus (Illkirch, France) and cAMP G_i kit from CisBio-PerkinElmer (Codolet, France).

Cell culture and transfection. CHO-K1 (ATCC, CCL-61) human CB₂R stable cell lines were cultured in Ham's F12 culture medium supplemented with 10% fetal bovine serum (FBS), 50 U/mL penicillin/streptomycin and 0.4 mg/mL geneticin (G418) and grown at 37°C and 5% CO₂. Cell transfection was performed with HEK293T cells (ATCC, CRL-3216) and jetPRIME transfection reagent according to the manufacturer's protocol.

Plant extraction. The extracts of *B. alba*, *C. ipecacuanha*, *C. limon*, *H. annuus*, *P. tomentosa*, *S. alba*, *S. kombe*, *V. odorata* and *V. tricolor* (Alfred Galke GmbH, Germany; *P. tomentosa* was collected in Costa Rica, at the tropical research station La Gamba) and peptide-enriched fractions thereof have been prepared as described previously¹⁸. Briefly, 50 g of dried plant material was extracted with 1 L of MeOH/DCM mixture (1:1, v/v) under continuous agitation at room temperature overnight. Plant material was removed by filtration and 0.5 volumes of water (ddH₂O) was added to the extract, to separate the aqueous MeOH phase containing peptides from organic phase. Prior to C₁₈ SPE the aqueous phase was evaporated and lyophilized, and the crude extract was dissolved in solvent A (99.9% ddH₂O, 0.1% TFA, v/v). The C₁₈ material ZEOprep 60 Å, irregular 40–64 μm (Zeochem, Uetikon, Switzerland) was equilibrated with solvent A and dissolved crude extract was loaded onto the C₁₈ cartridge. After washing with 10% - 30% of solvent B (90% AcN, 9.92% ddH₂O, 0.08% TFA, v/v/v) the peptide-containing fractions were eluted with 50% - 80% solvent B, optimized for each plant extract.

Peptide analysis with MALDI and ESI mass spectrometry. MALDI-TOF MS analysis of peptide-enriched fractions and synthesized cyclotide was performed on MALDI-TOF/TOF

4800 Analyser (AB Sciex, Framingham, MA, United States). MS and MS/MS spectra were recorded in a reflector positive ion mode acquiring 2,000 to 10,000 total shots per spectrum with a laser intensity of 3,500. Samples were prepared by mixing 3 μL of $\alpha\text{-CHCA}$ and 0.5 μL of peptide and spotting 0.5 μL of the mixture onto the MALDI 384 target plate. Spectra were acquired, processed, and analyzed using the Data Explorer SoftwareTM (AB Sciex, Framingham, MA, United States). The molecular weights of synthetic bicyclic peptides were analyzed by electrospray ionization mass spectrometry (ESI-MS) using a LCMS 2010 system (Shimadzu, Kyoto, Japan).

RP-HPLC fractionation and peptide purification. The pharmacology-guided fractionation of the *V. odorata* peptide-enriched extract and purification of synthesized peptides was performed as previously described¹⁸. In brief, the extract was dissolved in 5% solvent B and loaded onto the preparative Phenomenex Jupiter C₁₈ column (250 mm \times 21.2 mm, 10 μm , 300 \AA ; Phenomenex, Aschaffenburg, Germany). The mobile phase was composed of solvent A and solvent B. The automatic fractionation was performed on a Dionex 3000 LC machine (Dionex, Amsterdam, The Netherlands) using a linear gradient of solvent B between 5% and 65% at a flow rate of 8 mL/min. For analytical RP-HPLC runs, a Kromasil C₁₈ column (250 mm \times 4.6 mm, 5 μm , 100 \AA) and a Phenomenex Jupiter C18 column (150 \times 2 mm, 5 μm , 300 \AA) were used with applied linear gradient of solvent B between 5% and 65% and at a flow rate of 0.3 mL/min or 1 mL/min, respectively. The elution of peptides was monitored via UV absorbance at 214, 254, and 280 nm wavelengths.

Reduction, alkylation and proteolytic digestion for *de novo* sequencing. Disulfide bond reduction of purified peptide was carried out by adding DTT (final concentration 10 mM, pH 8.5) to an aliquot of peptide sample (5 μg) previously dissolved in 0.1 M NH_4HCO_3 followed by incubation for 3 h at 60°C. Cysteine residues were carbamidomethylated by adding IAA (final concentration 50 mM) to the reduced peptide sample and incubated for 1 min at 65°C. Prior enzymatic digestion, the reaction was terminated by adding DTT (final concentration 10 mM) and incubated for 10 min at room temperature. Reduced and alkylated peptide was proteolytically cleaved by adding either EndoGluC (0.5 μg) or trypsin (0.4 μg) and chymotrypsin (0.4 μg) and were incubated for 3 h at 37°C. The reaction was quenched by adding TFA (final concentration: 3%) to the samples. The masses of reduced, alkylated and digested peptides were monitored by MALDI mass spectrometry. The identified corresponding precursor masses derived from peptide digestion were used for MS/MS fragmentation experiments. Acquired MS spectra were analyzed, and peptides were manually sequenced by assembling fragments of identified N-terminal b-ions and C-terminal y-ions series. The identified amino acid sequence was confirmed by High Sensitivity Amino Acid Analysis (Macquarie University, Sydney, Australia).

Synthesis of vodo-C1 and bicyclic peptides. The cyclotide synthesis was carried out on an PTI Tribute Automatic Peptide Synthesizer (PTI Instruments, Boston, MA, United States) utilizing Fmoc chemistry as previously described⁶⁹. 2-chlorotrityl chloride resin was loaded with hydrazine, followed by the coupling of the first amino acid. Further coupling reactions were carried out with amino acids, 2-(1H-benzotriazol-1-yl)-1,1,3,3-tetramethyluronium-hexafluorophosphat and diisopropylethylamine for 30 min as well as 2 × 5 minutes Fmoc deprotection with 20% piperidine in dimethylformamide. The full-length precursor was obtained after cleavage from the resin in a mixture of TFA/triisopropylsilane/ddH₂O/1,2-ethanedithiol (92.5%/2.5%/2.5%/2.5%; v/v/v/v) for 4 h at room temperature. The freeze-dried hydrazine peptide was dissolved in 0.2 mM phosphate buffer (pH 3) at the concentration of 2 mM and the cyclization was initiated with sodium nitrite at -20°C for 15 min. The reaction was quenched with a 2-mercaptoethansulfonate solution in phosphate buffer (pH 7.5) to a final peptide solution of 0.2 mM for 4 h. The cyclic reduced peptide was purified via SPE C₁₈ and freeze dried. To obtain the native cystine knot, peptide was dissolved in the folding buffer consisting of 0.1 M NH₄HCO₃ (pH 8.4) / isopropanol (1:1, v/v), supplemented with the oxidative shuffling reagents reduced (2 mM) and oxidized (0.5 mM) glutathione at a concentration of 0.5 mg/mL. To quench the reaction, the buffered sample was acidified to pH of ~2 and freeze dried. The cyclic folded peptide was isolated with preparative HPLC, and the peptide purity was confirmed with analytical HPLC (214 nm) and MALDI. Vodo-C1 derived peptides were synthesized on a Microwave-Assisted Peptide Synthesizer (Liberty Prime, CEM) using a rink amide AM resin. Fmoc deprotection was done with 20 % piperidine in DMF for 1 min at 90°C. Amino acids were coupled in dicyclohexylcarbodiimide and ethyl cyanohydroxyiminoacetate (Oxyma), for 4 min at 90°C. Cyclization of bicyclic peptides was done as described previously⁴². Crude linear peptides were dissolved in buffer consisting of 70% (v/v) 20 mM NH₄HCO₃ (pH 8.0) and 30% (v/v) AcN and subjected for coupling reaction with 1,3,5-tris-(bromomethyl)-benzene for 1 h at room temperature. All peptides were purified using RP-HPLC, and peptide purity was confirmed with analytical HPLC runs at 0.3 and 1 mL/min. Correct peptide masses were confirmed with MALDI-MS or ESI-MS.

Radioligand binding assays. Radioligand binding assays using [³H]-CP55940 were carried out as described previously^{7,54}. Membranes were prepared using CHO-K1 cell line stably expressing human CB₂R according to previously published protocols⁷⁰. All experiments were performed in duplicates and binding buffer containing 50 mM Tris-HCl, 2.5 mM EDTA, 5 mM MgCl₂, 0.5 mg/mL fatty acid-free BSA (pH 7.4), in silanized glass vials. For competition binding, 75 µL each of [³H]-CP55940 (0.3-0.5 nM final), ligands (4X) and membranes (1-2 µg or 25 µg for CB₂R and CB₁R, respectively) were incubated for 2h at 30°C. To measure two-point radioligand displacement by bicyclic peptides we used mixture of radiolabeled (0.5 nM) and cold CP55940 (4.5 nM). Nonspecific binding of radioligand was determined in presence of AM630 or WIN55,212-2 at final concentration of 10 µM. After the incubation, membrane

suspensions were rapidly filtered through a 0.1% PEI-pres soaked GF/B glass fiber filters (Sartorius Stedim, Göttingen, Germany) with Skatron cell harvester (Skatron AS, Lier, Norway) and washed 3 times with ice-cold washing buffer containing 10 mM TRIS-HCl, 1 mM MgCl₂, 1 mg/mL fatty acid-free BSA (pH 7.7). The radioactivity retained on the filters was measured by liquid scintillation.

cAMP assay. The quantification of cAMP levels was carried out in triplicates with CHO-K1 cells stably expressing human CB₂R using the homogenous time-resolved fluorescence resonance energy transfer (HTRF) cAMP-Gi kit according to the manufacturer's instructions with minor modifications as described previously⁷¹. Briefly, 5,000 cells per 5 μ L per well were seeded into white 384-well plate and incubated with stimulation buffer (Opti-MEM media supplemented with 2% BSA and IBMX at 0.5 mM final concentration). Test compounds (4X) were diluted in stimulation buffer supplemented with 10 μ M forskolin to final solvent concentrations ranging from 0.03 – 30,000 nM and co-incubated with cells for additional 30 min at 37°C. To measure the allosteric modulation, the cells were pretreated with peptides (4X) for 30 min at 37°C followed by co-incubation of CP55940, WIN55,212-2 or 2-AG (4X) and forskolin for 30 min at 37°C. After the addition of 5 μ L Europium cryptate-labeled cAMP and cAMP d2-labeled antibody each and an incubation for 1 h at room temperature, fluorescence was measured at 620/665 nm using a Flexstation 3 plate reader (Molecular Devices, San Jose, USA). All measurements were performed with CP55940, WIN55,212-2 and/or 2-AG concentration-response curves as controls to assure cellular performance.

Data analysis. Data analysis was performed using GraphPad Prism (GraphPad Software, San Diego) and statistical analysis was performed by an unpaired t-test or one-way ANOVA. K_i values obtained from radioligand competition binding assays were determined by fitting the data to a three-parameter logistic Hill equation and applying the Cheng and Prusoff approximation⁷² by using a previously determined K_D of [³H]-CP55940 (0.5 nM)⁷. Data were normalized to specific binding of [³H]-CP55940 in absence of compounds as maximum percentage (100%), which refers to an average of 4,500-5,000 fmoles/mg protein for CB₂R and 250-350 fmoles/mg for CB₁R, respectively. To obtain dose response curves of functional assays, data were fitted to three-parameter non-linear regression curves with a bottom and top constrained to 0 and 100, respectively, and a slope of one to obtain potency (EC_{50}) and maximum efficacy (E_{max}). Concentration response curves of functional assays for measuring allosteric modulation were generated by fitting the data to three-parameter non-linear regression curves without constraints and a slope of one except for CP55940 which were constrained to zero (bottom) and hundred (top). Graphs were normalized to 100% which corresponds to the highest concentration of the positive control, which is either CP55940, WIN55,212-2 or 2-AG used in the assay. Concentration-response curves for the interaction between CP55940 or WIN55,212-2 and varying concentrations of each of vBCL1-4 in the

cAMP accumulation assay were globally fitted to the following simplified operational model of allostery and agonism, equation 1⁷³, where E_m denotes the maximum system response (efficacy).

$$\text{Equation 1: } E = \text{Basal} + \frac{(E_m - \text{Basal})([A](K_B + \alpha\beta[B] + \tau_B[B]EC_{50}))}{EC_{50}(K_B + [B]) + ([A](K_B + \alpha\beta[B]) + \tau_B[B]EC_{50})}$$

[A] and [B] are the concentrations of orthosteric agonist and allosteric ligand, respectively. K_B is the equilibrium dissociation constants of the allosteric ligand (vBCL1-4) and EC_{50} is the half maximal response of the orthosteric ligand. τ_B is the operational efficacy of the allosteric ligand. $\alpha\beta$ represents the composite of both binding and efficacy cooperativity factors between the orthosteric and allosteric ligands. Where K_B and $\alpha\beta$ values were estimated, the analysis fixed the transducer slope (n) to 1, the Basal to 0 and E_m to 100.

Cyclic peptide modelling with AlphaFold. 3D peptide structure predictions were performed as described previously³⁴. Briefly, AlphaFold was used combined with modified workflow that enhances the accuracy and confidence when predicting and designing cyclic peptides. The advanced protocol termed AfCycDesign utilizes a cyclic offset matrix. N- and C- terminus were manually connected using the CONECT syntax in the PDB file.

Molecular visualization and volume calculations. Peptide structures were visualized using PyMOL 2.5.5. Molecular volumes of compounds with a known 3D structure were calculated in UCSF ChimeraX 1.7 utilizing the built-in volume and area measuring tool. The volumes of molecules lacking 3D structure were calculated *via* Molinspiration's interactive property calculator⁷⁴.

Data availability. The data supporting this study are available from the corresponding author upon request. The cryo-EM structural data of CB₂R has been accessed via the Protein Data Bank (PDB) under accession code 6PT0, and the NMR structure of kalata B1 has been accessed via PDB accession code 1NB1.

AUTHOR INFORMATION

Corresponding author

Christian W. Gruber – Center for Physiology and Pharmacology, Institute of Pharmacology, Medical University of Vienna, 1090 Vienna, AUSTRIA; Email: christian.w.gruber@meduniwien.ac.at

Authors

Nataša Tomašević – Center for Physiology and Pharmacology, Institute of Pharmacology, Medical University of Vienna, 1090 Vienna, AUSTRIA

Fabiola Susanna Emser – Center for Physiology and Pharmacology, Institute of Pharmacology, Medical University of Vienna, 1090 Vienna, AUSTRIA

Jasmin Gattringer – Center for Physiology and Pharmacology, Institute of Pharmacology, Medical University of Vienna, 1090 Vienna, AUSTRIA

Simon Hasinger – Center for Physiology and Pharmacology, Institute of Pharmacology, Medical University of Vienna, 1090 Vienna, AUSTRIA

Roland Hellinger – Center for Physiology and Pharmacology, Institute of Pharmacology, Medical University of Vienna, 1090 Vienna, AUSTRIA

Peter Keov – Monash Institute of Pharmaceutical Sciences, Monash University, Parkville, VIC, 3052, Australia, and ARC Centre for Cryo-electron Microscopy of Membrane Proteins, Monash Institute of Pharmaceutical Sciences, Monash University, Parkville 3052, VIC, Australia

Manuel Felkl – Institute of Biological Chemistry, Faculty of Chemistry, University of Vienna, 1090 Vienna, AUSTRIA

Jürg Gertsch – Institute of Biochemistry and Molecular Medicine, University of Bern, 3012 Bern, SWITZERLAND

Christian F.W. Becker – Institute of Biological Chemistry, Faculty of Chemistry, University of Vienna, 1090 Vienna, AUSTRIA

Author contributions

C.W.G. designed research; N.T., F.S.E., J.G., R.H. and C.W.G. performed research; R.H. and M.F. synthesized peptides; C.F.W.B, J.G. and C.W.G. contributed new reagents/analytical tools; N.T., F.E., P.K., S.H., R.H. and C.W.G. analyzed data; N.T. and C.W.G. drafted the manuscript; all authors read and approved the final version of the manuscript.

ACKNOWLEDGMENTS

We thank Gaurav Bhardwaj & Stephen Rettie (University of Washington, USA) for help with structural modelling. Research in the laboratory of C.W.G. is funded by the Austrian Science Fund (FWF) through projects 10.55776/P36762 and 10.55776/P32109.

REFERENCES

1. Turcotte, C., Blanchet, M.-R., Laviolette, M. & Flamand, N. The CB2 receptor and its role as a regulator of inflammation. *Cell. Mol. Life Sci.* **73**, 4449–4470 (2016).
2. Guindon, J. & Hohmann, A. G. Cannabinoid CB2 receptors: a therapeutic target for the treatment of inflammatory and neuropathic pain. *Br. J. Pharmacol.* **153**, 319–334 (2008).
3. Whiting, Z. M., Yin, J., Harpe, S. M. de la, Vernall, A. J. & Grimsey, N. L. Developing the Cannabinoid Receptor 2 (CB2) pharmacopoeia: past, present, and future. *Trends Pharmacol. Sci.* **43**, 754–771 (2022).
4. Flipping the GPCR Switch: Structure-Based Development of Selective Cannabinoid Receptor 2 Inverse Agonists | Biological and Medicinal Chemistry | ChemRxiv | Cambridge Open Engage. <https://chemrxiv.org/engage/chemrxiv/article-details/653a546bc573f893f12245ba>.
5. Heimann, A. S. *et al.* Hemopressin as a breakthrough for the cannabinoid field. *Neuropharmacology* **183**, 108406 (2021).
6. Heimann, A. S. *et al.* Hemopressin is an inverse agonist of CB₁ cannabinoid receptors. *Proc. Natl. Acad. Sci.* **104**, 20588–20593 (2007).
7. Petrucci, V. *et al.* Pepcan-12 (RVD-hemopressin) is a CB2 receptor positive allosteric modulator constitutively secreted by adrenals and in liver upon tissue damage. *Sci. Rep.* **7**, 9560 (2017).
8. Muratspahić, E., Freissmuth, M. & Gruber, C. W. Nature-Derived Peptides: A Growing Niche for GPCR Ligand Discovery. *Trends Pharmacol. Sci.* **40**, 309–326 (2019).
9. Wang, L. *et al.* Therapeutic peptides: current applications and future directions. *Signal Transduct. Target. Ther.* **7**, 1–27 (2022).
10. Muratspahić, E. *et al.* Design and structural validation of peptide–drug conjugate ligands of the kappa-opioid receptor. *Nat. Commun.* **14**, 8064 (2023).
11. Congreve, M., de Graaf, C., Swain, N. A. & Tate, C. G. Impact of GPCR Structures on Drug Discovery. *Cell* **181**, 81–91 (2020).
12. Ballante, F., Kooistra, A. J., Kampen, S., Graaf, C. de & Carlsson, J. Structure-Based Virtual Screening for Ligands of G Protein–Coupled Receptors: What Can Molecular Docking Do for You? *Pharmacol. Rev.* **73**, 1698–1736 (2021).
13. Koehbach, J. *et al.* Oxytocic plant cyclotides as templates for peptide G protein-coupled receptor ligand design. *Proc. Natl. Acad. Sci.* **110**, 21183–21188 (2013).
14. Muratspahić, E. *et al.* Design of a Stable Cyclic Peptide Analgesic Derived from Sunflower Seeds that Targets the κ -Opioid Receptor for the Treatment of Chronic Abdominal Pain. *J. Med. Chem.* **64**, 9042–9055 (2021).
15. Ramiro, I. B. L. *et al.* Somatostatin venom analogs evolved by fish-hunting cone snails: From prey capture behavior to identifying drug leads. *Sci. Adv.* **8**, eabk1410 (2022).
16. Gertsch, J., Pertwee, R. G. & Di Marzo, V. Phytocannabinoids beyond the Cannabis plant – do they exist? *Br. J. Pharmacol.* **160**, 523–529 (2010).
17. Muratspahić, E., Koehbach, J., Gruber, C. W. & Craik, D. J. Harnessing cyclotides to design and develop novel peptide GPCR ligands. *RSC Chem. Biol.* **1**, 177–191 (2020).
18. Muratspahić, E. *et al.* Plant-Derived Cyclotides Modulate κ -Opioid Receptor Signaling. *J. Nat. Prod.* **84**, 2238–2248 (2021).
19. Taghizadeh, M. S. *et al.* Discovery of the cyclotide caripe 11 as a ligand of the cholecystinin-2 receptor. *Sci. Rep.* **12**, 9215 (2022).

20. Craik, D. J., Daly, N. L., Bond, T. & Waine, C. Plant cyclotides: A unique family of cyclic and knotted proteins that defines the cyclic cystine knot structural motif. *J. Mol. Biol.* **294**, 1327–1336 (1999).
21. Colgrave, M. L. & Craik, D. J. Thermal, Chemical, and Enzymatic Stability of the Cyclotide Kalata B1: The Importance of the Cyclic Cystine Knot. *Biochemistry* **43**, 5965–5975 (2004).
22. Aboye, T. *et al.* Design of a MCoTI-Based Cyclotide with Angiotensin (1-7)-Like Activity. *Molecules* **21**, 152 (2016).
23. Hellinger, R. *et al.* Peptidomics of Circular Cysteine-Rich Plant Peptides: Analysis of the Diversity of Cyclotides from *Viola tricolor* by Transcriptome and Proteome Mining. *J. Proteome Res.* **14**, 4851–4862 (2015).
24. Hellinger, R. *et al.* Peptidomics. *Nat. Rev. Methods Primer* **3**, 25 (2023).
25. Cheneval, O. *et al.* Fmoc-Based Synthesis of Disulfide-Rich Cyclic Peptides. *J. Org. Chem.* **79**, 5538–5544 (2014).
26. Koehbach, J. *et al.* Cyclotide discovery in Gentianales revisited—identification and characterization of cyclic cystine-knot peptides and their phylogenetic distribution in Rubiaceae plants. *Pept. Sci.* **100**, 438–452 (2013).
27. de Veer, S. J., Kan, M.-W. & Craik, D. J. Cyclotides: From Structure to Function. *Chem. Rev.* **119**, 12375–12421 (2019).
28. Conzelmann, C., Muratspahić, E., Tomašević, N., Münch, J. & Gruber, C. W. In vitro Inhibition of HIV-1 by Cyclotide-Enriched Extracts of *Viola tricolor*. *Front. Pharmacol.* **13**, 888961 (2022).
29. Lockett, S. *et al.* High-resolution structure of a potent, cyclic proteinase inhibitor from sunflower seeds¹ Edited by I. A. Wilson. *J. Mol. Biol.* **290**, 525–533 (1999).
30. Wang, C. K. L., Kaas, Q., Chiche, L. & Craik, D. J. CyBase: a database of cyclic protein sequences and structures, with applications in protein discovery and engineering. *Nucleic Acids Res.* **36**, D206-210 (2008).
31. Park, S. *et al.* Cyclotide Evolution: Insights from the Analyses of Their Precursor Sequences, Structures and Distribution in Violets (*Viola*). *Front. Plant Sci.* **8**, (2017).
32. Soethoudt, M. *et al.* Cannabinoid CB2 receptor ligand profiling reveals biased signalling and off-target activity. *Nat. Commun.* **8**, 13958 (2017).
33. Jumper, J. *et al.* Highly accurate protein structure prediction with AlphaFold. *Nature* **596**, 583–589 (2021).
34. Rettie, S. A. *et al.* Cyclic peptide structure prediction and design using AlphaFold. *BioRxiv Prepr. Serv. Biol.* 2023.02.25.529956 (2023) doi:10.1101/2023.02.25.529956.
35. Colgrave, M. L., Poth, A. G., Kaas, Q. & Craik, D. J. A new “era” for cyclotide sequencing. *Pept. Sci.* **94**, 592–601 (2010).
36. Nguyen, G. K. T. *et al.* Discovery and Characterization of Novel Cyclotides Originated from Chimeric Precursors Consisting of Albumin-1 Chain a and Cyclotide Domains in the Fabaceae Family. *J. Biol. Chem.* **286**, 24275–24287 (2011).
37. Mulvenna, J. P., Sando, L. & Craik, D. J. Processing of a 22 kDa Precursor Protein to Produce the Circular Protein Tricyclon A. *Structure* **13**, 691–701 (2005).
38. Zhang, J. *et al.* Identification of two suites of cyclotide precursor genes from metallophyte *Viola baoshanensis*: cDNA sequence variation, alternative RNA splicing and potential cyclotide diversity. *Gene* **431**, 23–32 (2009).
39. Simonsen, S. M. *et al.* A Continent of Plant Defense Peptide Diversity: Cyclotides in Australian *Hybanthus* (Violaceae). *Plant Cell* **17**, 3176–3189 (2005).

40. Eisenberg, D., Schwarz, E., Komaromy, M. & Wall, R. Analysis of membrane and surface protein sequences with the hydrophobic moment plot. *J. Mol. Biol.* **179**, 125–142 (1984).
41. Xing, C. *et al.* Cryo-EM Structure of Human Cannabinoid Receptor CB2-Gi Signaling Complex. *Cell* **180**, 645-654.e13 (2020).
42. Heinis, C., Rutherford, T., Freund, S. & Winter, G. Phage-encoded combinatorial chemical libraries based on bicyclic peptides. *Nat. Chem. Biol.* **5**, 502–507 (2009).
43. Seamon, K. B., Padgett, W. & Daly, J. W. Forskolin: unique diterpene activator of adenylate cyclase in membranes and in intact cells. *Proc. Natl. Acad. Sci. U. S. A.* **78**, 3363–3367 (1981).
44. Ross, R. A. *et al.* Agonist-inverse agonist characterization at CB1 and CB2 cannabinoid receptors of L759633, L759656 and AM630. *Br. J. Pharmacol.* **126**, 665–672 (1999).
45. Rinaldi-Carmona, M. *et al.* SR 144528, the First Potent and Selective Antagonist of the CB2 Cannabinoid Receptor. *J. Pharmacol. Exp. Ther.* **284**, 644–650 (1998).
46. Gonçalves, E. D. & Dutra, R. C. Cannabinoid receptors as therapeutic targets for autoimmune diseases: where do we stand? *Drug Discov. Today* **24**, 1845–1853 (2019).
47. Guindon, J. & Hohmann, A. G. The endocannabinoid system and cancer: therapeutic implication. *Br. J. Pharmacol.* **163**, 1447–1463 (2011).
48. Fahradsour, M. *et al.* Cyclotides Isolated from an Ipecac Root Extract Antagonize the Corticotropin Releasing Factor Type 1 Receptor. *Front. Pharmacol.* **8**, 616 (2017).
49. Hauser, A. S., Attwood, M. M., Rask-Andersen, M., Schiöth, H. B. & Gloriam, D. E. Trends in GPCR drug discovery: new agents, targets and indications. *Nat. Rev. Drug Discov.* **16**, 829–842 (2017).
50. Foster, S. R. *et al.* Discovery of Human Signaling Systems: Pairing Peptides to G Protein-Coupled Receptors. *Cell* **179**, 895-908.e21 (2019).
51. Muratspahić, E. *et al.* Genome Mining-Based Discovery of Blenny Fish-Derived Peptides Targeting the Mouse κ -Opioid Receptor. *Front. Pharmacol.* **12**, 773029 (2021).
52. Muratspahić, E. *et al.* Development of Melanocortin 4 Receptor Agonists by Exploiting Animal-Derived Macrocyclic, Disulfide-Rich Peptide Scaffolds. *ACS Pharmacol. Transl. Sci.* **6**, 1373–1381 (2023).
53. Raduner, S. *et al.* Alkylamides from Echinacea are a new class of cannabinomimetics. Cannabinoid type 2 receptor-dependent and -independent immunomodulatory effects. *J. Biol. Chem.* **281**, 14192–14206 (2006).
54. Gertsch, J. *et al.* Beta-caryophyllene is a dietary cannabinoid. *Proc. Natl. Acad. Sci.* **105**, 9099–9104 (2008).
55. Mahboubi, M. & Taghizadeh Kashani, L. M. A Narrative study about the role of *Viola odorata* as traditional medicinal plant in management of respiratory problems. *Adv. Integr. Med.* **5**, 112–118 (2018).
56. Alipanah, H., Bigdeli, M. R. & Esmaeili, M. A. Inhibitory Effect of *Viola odorata* Extract on Tumor Growth and Metastasis in 4T1 Breast Cancer Model. *Iran. J. Pharm. Res. IJPR* **17**, 276–291 (2018).
57. Ireland, D. C., Colgrave, M. L. & Craik, D. J. A novel suite of cyclotides from *Viola odorata*: sequence variation and the implications for structure, function and stability. *Biochem. J.* **400**, 1–12 (2006).
58. Jergova, S. *et al.* Cannabinoid receptor agonists from *Conus* venoms alleviate pain-related behavior in rats. *Pharmacol. Biochem. Behav.* **205**, 173182 (2021).
59. Hofer, S. C. *et al.* Localization and production of peptide endocannabinoids in the rodent CNS and adrenal medulla. *Neuropharmacology* **98**, 78–89 (2015).

60. Glasmacher, S. & Gertsch, J. Characterization of pepcan-23 as pro-peptide of RVD-hemopressin (pepcan-12) and stability of hemopressins in mice. *Adv. Biol. Regul.* **80**, 100808 (2021).
61. Bauer, M. *et al.* Identification and Quantification of a New Family of Peptide Endocannabinoids (Pepcans) Showing Negative Allosteric Modulation at CB1 Receptors. *J. Biol. Chem.* **287**, 36944–36967 (2012).
62. Luo, X. *et al.* Complete biosynthesis of cannabinoids and their unnatural analogues in yeast. *Nature* **567**, 123–126 (2019).
63. Pertwee, R. G. The diverse CB1 and CB2 receptor pharmacology of three plant cannabinoids: Δ 9-tetrahydrocannabinol, cannabidiol and Δ 9-tetrahydrocannabivarin. *Br. J. Pharmacol.* **153**, 199–215 (2008).
64. Laprairie, R. B., Bagher, A. M., Kelly, M. E. M. & Denovan-Wright, E. M. Cannabidiol is a negative allosteric modulator of the cannabinoid CB1 receptor. *Br. J. Pharmacol.* **172**, 4790–4805 (2015).
65. Thal, D. M., Glukhova, A., Sexton, P. M. & Christopoulos, A. Structural insights into G-protein-coupled receptor allostery. *Nature* **559**, 45–53 (2018).
66. Christopoulos, A. G Protein-Coupled Receptor Allostery and Complexing. *Pharmacol. Rev.* **54**, 323–374 (2002).
67. Gado, F. *et al.* Identification of the First Synthetic Allosteric Modulator of the CB2 Receptors and Evidence of Its Efficacy for Neuropathic Pain Relief. *J. Med. Chem.* **62**, (2018).
68. Shapiro, L., Gado, F., Manera, C. & Escayg, A. Allosteric modulation of the cannabinoid 2 receptor confers seizure resistance in mice. *Neuropharmacology* **188**, 108448 (2021).
69. Kremsmayr, T. *et al.* On the Utility of Chemical Strategies to Improve Peptide Gut Stability. *J. Med. Chem.* **65**, 6191–6206 (2022).
70. Nasrollahi-Shirazi, S. *et al.* Functional Impact of the G279S Substitution in the Adenosine A1-Receptor (A1R-G279S7.44), a Mutation Associated with Parkinson's Disease. *Mol. Pharmacol.* **98**, 250–266 (2020).
71. Li, X. *et al.* Crystal Structure of the Human Cannabinoid Receptor CB2. *Cell* **176**, 459-467.e13 (2019).
72. Cheng, Y. & Prusoff, W. H. Relationship between the inhibition constant (K₁) and the concentration of inhibitor which causes 50 per cent inhibition (I₅₀) of an enzymatic reaction. *Biochem. Pharmacol.* **22**, 3099–3108 (1973).
73. Aurelio, L. *et al.* Allosteric Modulators of the Adenosine A1 Receptor: Synthesis and Pharmacological Evaluation of 4-Substituted 2-Amino-3-benzoylthiophenes. *J. Med. Chem.* **52**, 4543–4547 (2009).
74. Molinspiration Cheminformatics. <https://www.molinspiration.com/>.